This is a preprint, the final version is subject to change, of the American Mineralogist (MSA)
Cite as Authors (Year) Title. American Mineralogist, in press.
(DOI will not work until issue is live.) DOI: http://dx.doi.org/10.2138/am-2017-6041

Revision 2

The crystal structure of turneaureite, $Ca_5(AsO_4)_3Cl$, the arsenate analogue of chlorapatite, and its relationships with the arsenate apatites johnbaumite and svabite

CRISTIAN BIAGIONI[1*], FERDINANDO BOSI[2,3], ULF HÅLENIUS[4], and MARCO PASERO[1]

[1] *Dipartimento di Scienze della Terra, Università di Pisa, Via S. Maria 53, I-56126 Pisa, Italy*

[2] *Dipartimento di Scienze della Terra, Sapienza Università di Roma, Piazzale Aldo Moro 5, I-00185 Roma, Italy*

[3] *CNR – Istituto di Geoscienze e Georisorse, UOS Roma, Piazzale Aldo Moro 5, I-00185 Roma, Italy*

[4] *Department of Geosciences, Swedish Museum of Natural History, Box 50007, SE-10405 Stockholm, Sweden*

**e-mail address: biagioni@dst.unipi.it*

ABSTRACT

The crystal structure of turneaureite, ideally $Ca_5(AsO_4)_3Cl$, was studied using a specimen from the Brattfors mine, Nordmark, Värmland, Sweden, by means of single-crystal X-ray diffraction data. The structure was refined to $R_1 = 0.017$ on the basis of 716 unique reflections with $F_o > 4\sigma(F_o)$ in the $P6_3/m$ space group, with unit-cell parameters $a = 9.9218(3)$, $c = 6.8638(2)$ Å, $V = 585.16(4)$ Å^3. The chemical composition of the sample, determined by electron-microprobe analysis, is (in wt% - average of 10 spot analyses): SO_3 0.22, P_2O_5 0.20, V_2O_5 0.01, As_2O_5 51.76, SiO_2 0.06, CaO 41.39, MnO 1.89, SrO 0.12, BaO 0.52, PbO 0.10, Na_2O 0.02, F 0.32, Cl 2.56, H_2O_{calc} 0.58, O (≡ F+Cl) –0.71, total 99.04. On the basis of 13 anions per formula unit, the empirical formula corresponds to $(Ca_{4.82}Mn_{0.17}Ba_{0.02}Sr_{0.01})_{\Sigma 5.02}(As_{2.94}P_{0.02}S_{0.02}Si_{0.01})_{\Sigma 2.99}O_{12}[Cl_{0.47}(OH)_{0.42}F_{0.11}]_{\Sigma 1.00}$.

Turneaureite is topologically similar to the other members of the apatite supergroup: columns of face-sharing *M*1 polyhedra running along **c** are connected through TO_4 tetrahedra with channels hosting *M*2 cations and *X* anions. Owing to its particular chemical composition, the studied turneaureite can be considered as a ternary calcium arsenate apatite; consequently it has several partially-filled anion sites within the anion columns. Polarised single-crystal FTIR spectra of the studied sample indicate stronger hydrogen bonding and less diverse short-range atom arrangements around (OH) groups in turneaureite as compared to the related minerals johnbaumite and svabite. An accurate knowledge of the atomic arrangement of this apatite-remediation mineral represents an improvement in our understanding of minerals able to sequester and stabilize heavy metals such as arsenic in polluted areas.

Key-words: turneaureite, calcium arsenate, apatite supergroup, crystal structure, infrared spectroscopy, Sweden.

Introduction

Calcium arsenate apatites belong to the apatite supergroup, a series of minerals having the general formula $^{IX}M1_2{}^{VII}M2_3(^{IV}TO_4)_3X$ (Pasero et al. 2010). Three calcium arsenate members are known: johnbaumite, svabite, and turneaureite, differing for the nature of the X anion, that is $(OH)^-$, F^-, and Cl^- respectively. Whereas the crystal structures of johnbaumite and svabite were recently investigated (Biagioni and Pasero 2013; Biagioni et al. 2016), the structural features of turneaureite have not been described so far, even if the crystal structure of synthetic $Ca_5(AsO_4)_3Cl$ was reported by Wardojo and Wu (1996). In addition, natural specimens of turneaureite usually show a complex anion composition, allowing a better understanding of the crystal chemistry of binary and ternary calcium arsenate apatites. Indeed, whereas binary and ternary calcium phosphate apatites have been accurately studied (e.g., Hughes et al. 1989, 1990, 2014), few data are available for their arsenate analogues. This paper aims at filling this gap.

Turneaureite was first described by Dunn et al. (1985) from three different localities, i.e. Franklin, New Jersey, USA; Balmat, New York, USA; and Långban, Värmland, Sweden, as the arsenate analogue of chlorapatite, $Ca_5(PO_4)_3Cl$, and the calcium analogue of mimetite, $Pb_5(AsO_4)_3Cl$. Only the specimen from the Swedish locality allowed the full-characterization of the species and was designated as the holotype. Although the symmetry of apatites is typically hexagonal (space group $P6_3/m$), several phases have been reported with lower symmetry (e.g., White et al. 2005; Baikie et al. 2007), sometimes showing superstructure reflections (e.g., Chackmouradian and Medici 2005). This is particularly true for Cl-bearing apatites. As a matter of fact neither deviation from the hexagonal symmetry nor any superstructure reflections in turneaureite were reported by Dunn et al. (1985). The specimen from Långban has chemical composition $(Ca_{4.85}Mn_{0.16}Pb_{0.02})_{\Sigma 5.03}[(AsO_4)_{2.42}(PO_4)_{0.54}]_{\Sigma 2.96}(Cl_{0.56}F_{0.39})_{\Sigma 0.95}$, with unit-cell parameters a = 9.810(4), c = 6.868(4) Å, V = 572.4 Å^3. The crystal structure of synthetic $Ca_5(AsO_4)_3Cl$ was refined by Wardojo and Hwu (1996) in the space group $P6_3/m$, with unit-cell

parameters a = 10.076(1), c = 6.807(1) Å, V = 598.4 Å^3. Dai and Harlow (1991) presented, as a communication at a meeting, the results of the single-crystal X-ray diffraction study for the three natural calcium arsenate apatites, but to our knowledge the results of their work were never published.

Owing to the fact that an understanding of the crystal structure of As-rich minerals is useful in environmental remediation (e.g., Rakovan and Pasteris 2015), we carried out a combined chemical, structural, and spectroscopic study of turneaureite from Nordmark, Värmland, Sweden. The present data, in conjunction with data from johnbaumite and svabite (Biagioni and Pasero 2013; Biagioni et al. 2016), provide the basis for a comparative analysis of the crystal-chemical features of the three calcium arsenate minerals with the apatite structure.

Experimental

The studied specimen (catalogue number NRM19532695) is from the Brattfors mine (latitude 59.83°N, longitude 14.12°E), Nordmark ore field, Filipstad, Värmland, Sweden. In this area there are about twenty small mines and prospects, which have been worked mainly for magnetite ore (e.g., Magnusson, 1929). The studied specimen of turneaureite consists of a fine-grained, irregularly fine-banded, metamorphosed siliceous carbonate rock, mainly composed of Mn-bearing calcite. Alleghanyite, jacobsite, and tephroite occurs as small (<0.5 mm) rounded grains together with katoptrite and turneaureite in the calcite matrix. Grains of turneaureite (up to 3 mm) are rounded or short prismatic to almost fibrous in habit, whereas katoptrite grains (up to 2 mm long) are typically lath-shaped. Very rare rounded grains (< 1mm) of magnussonite are also observed. Dark red aggregates of alleghanyite cover up to 1 cm^2 large areas in some micro-fissures.

Electron microprobe analyses were obtained by wavelength dispersive spectroscopy (WDS mode) with a Cameca SX50 instrument at the “Istituto di Geologia Ambientale e Geoingegneria,

CNR" of Rome, Italy, using the following analytical conditions: accelerating voltage 15 kV, beam current 15 nA, nominal beam diameter 1 μm. Counting time for one spot analysis was 20 s per peak. Standards (element, emission line) are: baryte (Ba*L*α, S*K*α), apatite (P*K*α), GaAs (As*L*α), wollastonite (Ca*K*α, Si*K*α), vanadinite (V*K*α), rhodonite (Mn*K*α), celestine (Sr*K*α), galena (Pb*M*α), jadeite (Na*K*α), phlogopite (F*K*α), and sylvite (Cl*K*α). The PAP routine was applied (Pouchou and Pichoir 1991) for correction of recorded raw data. Ten spot analyses were performed; the studied grain was found to be homogeneous. Chemical data are given in Table 1; the chemical formula, based on 13 anions per formula unit, is $(Ca_{4.82}Mn_{0.17}Ba_{0.02}Sr_{0.01})_{\Sigma 5.02}(As_{2.94}P_{0.02}S_{0.02}Si_{0.01})_{\Sigma 2.99}O_{12}[Cl_{0.47}(OH)_{0.42}F_{0.11}]_{\Sigma 1.00}$.

Polarised single-crystal infrared spectra of turneaureite were recorded with a Bruker Vertex 70 microscope spectrometer equipped with a halogen lamp source, a KBr beam-splitter, a holographic ZnSe polarizer, and a midband MCT detector. The crystal was oriented by morphology and optical microscopy and was doubly polished parallel to the **a-c** axis plane. The thickness of the single crystal absorber was 38 μm. Polarized absorption spectra were acquired parallel (E||E) and perpendicular (E||O) to the **c**-axis over the wavenumber range 600–5000 cm^{-1} with a resolution of 2 cm^{-1} during 32 cycles. The spectral region of the O–H stretching bands of the recorded single-crystal spectra was fitted using the *PeakFit* 4.12 software (Jandel) assuming Gaussian peak shapes.

A crystal fragment (230 × 230 × 100 μm in size) was selected for the single-crystal X-ray diffraction study. Intensities were collected using a Bruker Smart Breeze diffractometer (50 kV, 30 mA) equipped with a CCD 4k low-noise area detector. Graphite-monochromatized Mo*K*α radiation was used. The detector-to-crystal working distance was 50 mm. 558 frames were collected in ω and φ scan modes in 0.5° slices; the exposure time was 10 s per frame. The data were integrated and corrected for Lorentz and polarization, background effects, and absorption using the package of softwares *Apex*2 (Bruker AXS Inc. 2004), resulting in a set of 753 independent reflections. The refinement of unit-cell parameters constrained to hexagonal symmetry gave a = 9.9218(3), c =

118 6.8638(2) Å, V = 585.16(4) Å^3. The statistical tests on the distribution of $|E|$ values ($|E^2 - 1|$ =
119 1.019) and the systematic absences suggested the space group $P6_3/m$.

120 The crystal structure was refined starting from the atomic coordinates of chlorapatite (Hughes
121 et al. 1989) using *Shelxl*-2014 (Sheldrick 2015). Scattering curves for neutral atoms were taken
122 from the International Tables for Crystallography (Wilson 1992). The site occupation factors (s.o.f.)
123 of the three cation and four anion sites were initially refined using the following scattering curves:
124 Ca at the *M*1 and *M*2 sites; As at the *T* site; O at the O1, O2, O3 sites and Cl at the *X* site. Owing to
125 the complex anion chemistry, the position of the latter site was found through difference-Fourier
126 map that showed the presence of a maximum at (0, 0, ¼). After a few cycles of isotropic
127 refinement, the R_1 converged to 0.079. In order to account for the occurrence of other elements
128 substituting for Ca, the s.o.f. of *M*1 and *M*2 were refined using the scattering curves of Ca *vs* Mn
129 and Ca *vs* Ba respectively. Only a minor improvement of the refinement was observed. After the
130 introduction of the anisotropic displacement parameters for cations, the R_1 converged to 0.054.
131 Assuming an anisotropic model also for the O1, O2, and O3 positions, the R_1 value converged to
132 0.047. The displacement parameter of the X anion was refined isotropically. Indeed, the anisotropic
133 refinement of the displacement parameter of the X anion resulted in a very high U value [in
134 particular U^{33}, i.e. 0.262(6) Å^2], suggesting the replacement of Cl by lighter atoms (in agreement
135 with chemical data) and the structural disorder affecting the column anions. Likely, these high
136 values of the anisotropic displacement parameters could mask the occurrence of several partially
137 occupied positions along the columns. Consequently, notwithstanding the good R value obtained
138 using an anisotropic description of the displacement parameter of the *X* position (i.e. R_1 = 0.023), an
139 isotropic model was preferred. In this way, a very high residual of 7.5 e/Å^3 at (0, 0, 0.33) was
140 found. By adding this additional position (named *X*b), constraining the isotropic U value of *X*a and
141 *X*b to be equal, and freely refining their s.o.f., the R_1 converged to 0.018. The refined site scattering
142 indicated the occurrence of about 5.5 and 7.8 electrons per formula unit at *X*a and *X*b, respectively.

The *X*b position was assumed to be occupied by Cl only, owing to the longer *M*2–*X*b distance, whereas *X*a was assumed to have a mixed (OH, Cl, F) occupancy. The proposed site population, taking into account the site multiplicity, was ($OH_{0.42}F_{0.11}Cl_{0.06}$) and $Cl_{0.41}$ at *X*a and *X*b, respectively. The highest maximum residual was 1.14 $e/Å^3$ at (0, 0, 0.40); this position is similar to the split Cl site found by Hughes et al. (1990) in ternary apatites. Consequently, we added this further position, labeled as *X*c, assuming for it a partial occupancy by Cl only, and removing the minor amount of this element from the *X*a site. The refinement converged to $R_1 = 0.0172$ for 716 unique reflections with $F_o > 4\ \sigma(F_o)$ (0.0185 for all 753 reflections) and 42 refined parameters. The chemical formula derived from the structure refinement (SREF) is $(Ca_{4.92}Ba_{0.05}Mn_{0.03})(AsO_4)_3[Cl_{0.47}(OH)_{0.42}F_{0.11}]$. Details of data collection and refinement are given in Table 2. Fractional atom coordinates, site occupancy factors, and isotropic or equivalent isotropic displacement parameters are reported in Table 3, whereas Table 4 gives anisotropic displacement parameters. Finally, Table 5 reports selected bond distances, and Table 6 shows the bond-valence calculations obtained using the bond-valence parameters of Brese and O'Keeffe (1991).

Crystal structure description

General features, cation coordination, and site population

The crystal structure of turneaureite is topologically similar to those of the other members of the apatite supergroup. It is composed by columns of face-sharing *M*1-centered polyhedra running along **c**; those polyhedra can be described as tricapped trigonal prisms. Adjacent columns are connected by TO_4 tetrahedra through corner-sharing. The *M*1 and *M*2 sites are Ca-dominant sites, with only a minor replacement by other cations, in agreement with chemical data. Refined site scattering at *M*1 (20.0 electrons) suggests only negligible replacement by heavier elements; consequently this site has a virtually pure Ca site population. The average <*M*1–O> distance is

2.579 Å, to be compared with 2.584 Å reported by Wardojo and Hwu (1996) for synthetic $Ca_5(AsO_4)_3Cl$ and 2.549 Å for chlorapatite studied by Hughes et al. (1989). Bond valence sum (BVS) at *M*1, calculated using the proposed site population, is 1.98 valence units (v.u.). The *M*2 site has a seven-fold coordination, with <*M*2–φ> = 2.529 Å, compared with 2.505 and 2.493 Å for synthetic $Ca_5(AsO_4)_3Cl$ and chlorapatite, respectively. The *M*2 site scattering (20.7 electrons) agrees with the site population ($Ca_{0.93}Mn_{0.06}Ba_{0.01}$). The BVS at *M*2 is 2.00 v.u. The site population of the *M*1+*M*2 sites, taking into account the site multiplicity, is consistent with ($Ca_{4.79}Mn_{0.18}Ba_{0.03}$), in agreement with electron-microprobe data. Finally, the *T* site is occupied by As^{5+}, with minor substitutions of P^{5+}, S^{6+}, and Si^{4+}. The average <*T*–O> distance is 1.678 Å, a little longer than the bond distances observed in johnbaumite and svabite (1.671 and 1.674 Å, respectively; Biagioni and Pasero 2013; Biagioni et al. 2016) and close to that reported for synthetic $Ca_5(AsO_4)_3Cl$ (1.682 Å) by Wardojo and Hwu (1996) and for johnbaumite from Franklin (1.70 Å) by Henderson et al. (2009). The BVS at *T* is 5.10 v.u..

The anion columns

The studied specimen can be classified as turneaureite, because Cl is the dominant column anion. Actually, this sample could be defined as a ternary calcium arsenate apatite, with chemical composition $Turn_{47}John_{42}Svab_{11}$.

Three sites in the [001] columns were located, at coordinates (0, 0, ¼), (0, 0, 0.31), and (0, 0, 0.37). Whereas in end-member (OH)-apatites, the hydroxyl group is displaced from the (0, 0, ¼) position, being disordered 0.35 Å above or below the mirror plane (e.g., Hughes et al. 1989; Biagioni and Pasero 2013), in turneaureite the (OH) groups have been located at the *X*a position lying on the mirror plane. A minor substitution of (OH) by F is proposed. The *X*b and *X*c site have been assumed to be occupied by Cl only. Actually, such split sites are inserted to model an electron density that is continuously distributed along the anion column and around the mirror plane, constrained by the necessity to avoid unrealistically short anion–anion distances.

In any column, there are five possible anion sites: i) *X*a, located on the mirror plane, ii, iii) *X*b, located 0.38 Å above (hereafter Xb_a, where subscript *a* stands for above) and 0.38 Å below (Xb_b where subscript *b* stands for below) the mirror plane, and iv, v) *X*c, located 0.83 Å above (Xc_a) and below (Xc_b) the mirror plane. Figure 1 show the anion–anion distances in the studied turneaureite. Owing to the necessity to avoid short anion–anion contacts, only some configurations are possible, confirming that complete disordering along anion columns is not realistic. Consequently, there could be anion ordering within individual columns and disordering among the column themselves, thus giving rise to completely disordered hexagonal structures (e.g., Hughes et al. 1989).

Bond strain analysis

Bosi (2014) demonstrated the occurrence of systematic errors in bond valence calculations incident at the mixed occupancy sites. This type of error is very invidious because can give rise to a false indication of the presence of steric strain. However, as the systematic errors introduced into the weighted BVS of turneaureite (Table 6) have been estimated to be small (< 0.05 v.u.), the difference between BVS and expected weighted atomic valence can be interpreted in terms of bond strain (Brown 2016). In detail, the anions at *X*a may be considered as underbonded, because its BVS is smaller than the expected value (0.33 v.u. and 0.53 v.u., respectively). On the other hand, *X*b may be considered as overbonded, because its BVS is larger than the expected value (0.75 v.u. and 0.41 v.u., respectively). Regarding the *X*c site, its BVS agrees with the expected value (0.06 v.u.). The above-mentioned deviations (bond strain) from the expected bond valence sum values are likely related to the disorder in the actual position of the column anions and possibly to the unresolved splitting of the *M*2 site.

Discussion

Chlorine position in turneaureite

Hughes et al. (1989) determined the anion positions in end-member calcium phosphate apatites and postulated that the anion positions in binary and ternary (F-OH-Cl) apatites would be impossible to predict. Indeed, in agreement with these authors, an extensive rearrangement of the end-member anion configurations may occur in ternary apatites in order to accommodate the large Cl^- anion. In chlorapatite, Cl is located at (0, 0, 0.44), 1.2 Å above and below the mirror plane located at (0, 0, ¼) (Hughes et al. 1989); in synthetic $Ca_5(AsO_4)_3Cl$, Cl is at (0, 0, 0.37), 0.84 Å above and below the mirror plane (Wardojo and Hwu 1996). In ternary phosphate apatites, a 0.4 Å shift of the Cl^- anion toward the mirror plane was observed by Hughes et al. (1990). Such a shift is accompanied by a splitting of the *M*2 position as a function of the neighboring anion to which *M*2-hosted cation is bonded. In some cases, the ordering of Cl and (OH) in anion columns could result in a lowering of symmetry, from $P6_3/m$ to $P2_1/b$ with a doubling of the **b** axis (Chakhmouradian and Medici 2006).

In the turneaureite studied, only the first phenomenon, i.e. the shift of Cl, occurs, whereas no hints of the occurrence of a doubling of the *b* parameter were observed. The splitting of the *M*2 site was not resolved, even if the U^{22} value is definitely larger than the corresponding value at *M*1 and those reported for *M*2 sites in johnbaumite and svabite (Biagioni and Pasero 2013; Biagioni et al. 2016), thus suggesting a possible positional disorder of this site in the {0001} plane.

In the studied sample, Cl is mainly located at (0, 0, 0.31), corresponding to a shift of 0.44 Å with respect to the Cl position in synthetic $Ca_5(AsO_4)_3Cl$. Another split position, having a low s.o.f., occurs at (0, 0, 0.37), corresponding to the coordinates of the Cl in the synthetic compound. This behavior is similar to that reported by Hughes et al. (1990) during their study of ternary apatites. Indeed they located Cl at (0, 0, 0.368), shifted 0.4 Å towards the mirror plane with respect to near-to-end-member chlorapatite; in addition, they found another split site, having a low site occupancy, at coordinates corresponding to that of Cl in chlorapatite, i.e. (0, 0, 0.44).

The Ca–Cl distances in turneaureite, i.e. 2.57 (*M*2–*X*b) and 2.67 Å (*M*2–*X*c), are similar to those given by Hughes et al. (1990) for ternary apatites, i.e. 2.63 and 2.70 Å for the two split *Ca*2 positions, in keeping with the chemical complexity of the turneaureite studied. These distances are definitely shorter than those reported for synthetic $Ca_5(AsO_4)_3Cl$ and for chlorapatite, both showing Ca–Cl distances of ~2.76 Å (Hughes et al. 1989; Wardojo and Hwu 1996), in keeping with the shift of Cl toward the mirror plane in apatites having a complex anion chemistry and the unresolved splitting of the *M*2 site.

Comparison with johnbaumite and svabite

The refinement of the crystal structure of turneaureite, in conjunction with data from Biagioni and Pasero (2013) and Biagioni et al. (2016), completes the triptych of natural calcium arsenate apatites, allowing important comparison of their structural features.

Natural samples generally have non-ideal (non-end-member) compositions. Indeed, only the johnbaumite composition studied by Biagioni and Pasero (2013) was close to the ideal $Ca_5(AsO_4)_3(OH)$ formula, having only negligible amounts of Cl and with F being below the detection limit. The sample of svabite, on the contrary, contains significant amounts of (OH) replacing F. Concerning cation substitutions, Ca was replaced by Pb and Mn only in svabite and turneaureite, respectively. Phosphorus-to-arsenic substitution is trivial in all the studied samples (up to 0.04 apfu in johnbaumite).

Unit-cell parameters of johnbaumite and svabite are similar, with a = 9.72, c = 6.96 Å, V = 570.4 Å^3 for the former and a = 9.73, c = 6.98 Å, V = 572.1 Å^3 for the latter. The unit-cell volume increase of svabite is only related to minor Pb replacing Ca. Indeed, the size of $(OH)^-$ is slightly larger than F^- and consequently the unit-cell volume of johnbaumite should be larger than that of svabite. The unit-cell volume of turneaureite is significantly larger, i.e. 585.2 Å^3 (ΔV = +2.3 and +2.6% with respect to svabite and johnbaumite, respectively). Notably there is an expansion of the a parameter (a = 9.92 Å, Δa ~ +2%) accompanied by a contraction of the c parameter (c = 6.86 Å,

265 $\Delta c \sim -1.6\%$); this behavior is more evident in synthetic $Ca_5(AsO_4)_3Cl$, having a = 10.076 Å ($\Delta a \sim$
266 +3.5%) and c = 6.807 ($\Delta c \sim -2.3\%$). This could accommodate an increase in the diameter of the
267 anion columns (Fig. 2), favoring the accommodation of the large Cl^- anion, as indicated by the
268 larger *M*2–*M*2 distance in turneaureite (4.40 Å) with respect to those observed in johnbaumite and
269 svabite (4.11-4.12 Å). Indeed, as the size of the X anion increases, the tunnels become wider
270 through reduction in the metaprism twist angle φ (e.g., White and Dong 2003; White et al. 2005),
271 defined as the angle O1–*M*1–O2 projected on (001) (White and Dong 2003; Lim et al. 2011). This
272 angle is used for the assessment of the distortion of the apatite structure from an ideal hexagonal
273 close packing of oxygen atoms. The metaprism twist angle in turneaureite, calculated according to
274 the formula proposed by Henderson et al. (2009), is 16.4°, definitely smaller than the corresponding
275 angles observed in johnbaumite (21.1°, Biagioni and Pasero 2013) and svabite (21.5°, Biagioni et
276 al. 2016), in agreement with the expansion of the anion columns in the (001) plane.

277 **Fourier Transform Infrared Spectroscopy (FTIR) of turneaureite**

278 The infrared spectra of turneaureite are very similar to those reported for svabite and
279 johnbaumite (Biagioni et al. 2016) and display strong absorption bands related to vibrational modes
280 in AsO_4-tetrahedra in the range 750-950 cm^{-1} and distinct absorption related to O–H stretching
281 modes in the range 3450-3600 cm^{-1}. As in spectra of the related minerals, the O–H stretching band
282 is polarized in E||**c** because of O–H dipole alignments along the crystallographic **c** axis. The
283 recorded FTIR E||**c** (E||E) spectrum of turneaureite in the O–H stretching region is compared with
284 those of svabite and johnbaumite in Figure 3. Whereas the positions of the O–H stretching bands
285 are almost identical in svabite and johnbaumite (Biagioni et al. 2016), they are shifted towards
286 lower wavenumbers by 5-15 cm^{-1} in turneaureite, thus indicating stronger hydrogen bonding. In
287 addition, the intensity of the high-energy component of the O–H stretching region observed in
288 spectra of johnbaumite and svabite at ~3560 cm^{-1} is strongly reduced in the turneaureite spectra.
289 This suggests less diverse short-range atom arrangements around the (OH) groups in turneaureite

compared to the two related minerals. Using the IR method for determining the (OH) concentration in apatite (Wang et al. 2011), the H_2O content in the turneaureite specimen should be close to 0.28 wt%, which is lower than the 0.58 wt% calculated for the empirical formula on the basis of electron-microprobe analysis. As in svabite and johnbaumite (Biagioni et al. 2016), the calculated H_2O concentration is approximately one half of that estimated from chemical data.

Implications

The refinement of the crystal structure of turneaureite through single-crystal X-ray diffraction using a natural specimen from Sweden has a two-fold relevance, i) adding new data to the knowledge of the crystal chemistry of calcium arsenate apatites, and ii) giving further insights into the complex anion arrangement in anion columns owing to its complex chemistry.

The occurrence of arsenic in surface and groundwaters in several localities world-wide (e.g., in south-eastern Asia; Charlet and Polya 2006) and its observed adverse health effects emphasize the importance of calcium arsenate apatites, owing to their potential role as sequestrators and stabilizers of arsenic from polluted water (e.g., Magalhães and Williams 2007; Liu et al. 2014). In order to explore their possible application in environmental remediation (e.g., Rakovan and Pasteris 2015), a deep knowledge of their crystal chemistry is mandatory, because the atomic arrangement of their crystal structure strongly affects their physical properties. Although several high-quality crystal structure refinements are available for calcium phosphate apatites (e.g., White et al. 2005), only a few investigations through single-crystal X-ray diffraction have been reported so far for the corresponding arsenate analogs. Recently, Biagioni and Pasero (2013) and Biagioni et al. (2016) gave the first structural data obtained through single-crystal techniques on natural samples of $Ca_5(AsO_4)_3OH$ (johnbaumite) and $Ca_5(AsO_4)_3F$ (svabite). As stated above, the refinement of the crystal structure of turneaureite completes the triptych of natural calcium arsenate apatites, improving the knowledge of the crystal chemistry of this group.

315 In addition, the complex anion chemistry of the turneaureite studied in this work, showing the
316 simultaneous presence of Cl, (OH), and minor F as column anions, is particularly intriguing.
317 Indeed, apatites are among the few minerals showing anion substitution series. Owing to the
318 different sizes of the three column anions F, (OH), and Cl, as well as to the steric interactions
319 among those anions in the anion columns, particularly complex atomic arrangements could result.
320 As stressed by Hughes et al. (2014), despite the widespread interest in apatites and the dependence
321 of all their properties on the atomic arrangements, the crystal structures of binary and ternary
322 apatites are not well understood as the anion distribution is not predictable from the structures of
323 end-members. Consequently, several studies have been focused on the atomic arrangements in the
324 anion columns (e.g., Hughes 2015). With respect to synthetic $Ca_5(AsO_4)_3Cl$ (Wardojo and Hwu
325 1996), where only Cl was present, the studied turneaureite represents a ternary arsenate apatite that
326 offers the possibility to describe the anion substitution series between turneaureite itself and the two
327 other arsenate apatites (johnbaumite and svabite). The results show a Cl shifting toward the mirror
328 planes, similar to that reported in ternary calcium phosphate apatites (Hughes et al. 1990).
329 As the understanding of these anion substitutions is more than an academic exercise (Hughes
330 and Rakovan 2015), being essential to take into account several scientific aspects (e.g., the volatile
331 behavior and budgets in melts and related fluids) as well as technological properties of apatites, the
332 present study represents a further step in the knowledge of the atomic arrangements and chemical
333 substitution mechanisms of this important supergroup of minerals.
334

335 ## Acknowledgments

336 We wish to thank Marcello Serracino who assisted us during electron-microprobe analysis.
337 MP acknowledges the financial support from the University of Pisa (PRA_2015_0028). Fernando
338 Cámara, Anthony R. Kampf and an anonymous reviewer helped us improving the paper.
339

References

Baikie, T., Mercier, P.H.J., Elcombe, M.M., Kim, J.Y., Le Page, Y., Mitchell, L.D., White, T.J. and Whitfield, P.S. (2007) Triclinic apatites. Acta Crystallographica, B63, 251-256.

Biagioni, C., and Pasero, M. (2013) The crystal structure of johnbaumite, $Ca_5(AsO_4)_3OH$, the arsenate analogue of hydroxylapatite. American Mineralogist, 98, 1580-1584.

Biagioni, C., Bosi, F., Hålenius, U., and Pasero, M. (2016) The crystal structure of svabite, $Ca_5(AsO_4)_3F$, an arsenate member of the apatite supergroup. American Mineralogist, 101, 1750-1755.

Bosi, F. (2014) Bond valence at mixed occupancy sites. I. Regular polyhedra. Acta Crystallographica, B70, 864–870.

Brese, N.E., and O'Keeffe, M. (1991) Bond-valence parameters for anion-anion bonds in solids. Acta Crystallographica, B48, 152-154.

Brown, I.D. (2016) The chemical bond in inorganic chemistry: the bond valence model. Series: International Union of Crystallography Monographs on Crystallography, 12, Oxford University Press, UK, 352 pp.

Bruker AXS Inc. (2004) APEX 2. Bruker Advanced X-ray Solutions, Madison, Wisconsin, USA.

Chakhmouradian, A.R., and Medici, L. (2006) Clinohydroxylapatite: a new apatite-group mineral from northwestern Ontario (Canada), and new data on the extent of Na-S substitution in natural apatites. European Journal of Mineralogy, 18, 105-112.

Charlet, L., and Polya, D.A. (2006) Arsenic in shallow, reducing groundwaters in Southern Asia: an environmental health disaster. Elements, 2, 91-96.

Dai, Y.S., and Harlow, G.E. (1991) Structural relationships of arsenate apatites with their anion-devoid intermetallic phase Ca_5As_3. Geological Society of America Annual Meeting, Program and Abstracts, 23, A219.

364 Dunn, P.J., Petersen, E.U., and Peacor, D.R. (1985) Turneaureite, a new member of the apatite
365 group from Franklin, New Jersey, Balmat, New York and Långban, Sweden. Canadian
366 Mineralogist, 23, 251-254.
367 Henderson, C.M.B., Bell, A.M.T., Charnock, J.M., Knight, K.S., Wendlandt, R.F., Plant, D.A., and
368 Harrison, W.J. (2009) Synchrotron X-ray absorption spectroscopy and X-ray powder
369 diffraction studies of the structure of johnbaumite [$Ca_{10}(AsO_4)_6(OH,F)_2$] and synthetic Pb-,
370 Sr- and Ba-arsenate apatites and some comments on the crystal chemistry of the apatite
371 structure type in general. Mineralogical Magazine, 73, 433-455.
372 Hughes, J.M. (2015) The many facets of apatite. American Mineralogist, 100, 1033-1039.
373 Hughes, J.M., and Rakovan, J.F. (2015) Structurally robust, chemically diverse: apatite and apatite
374 supergroup minerals. Elements, 11, 165-170.
375 Hughes, J.M., Cameron, M., and Crowley, K.D. (1989) Structural variation in natural F, OH, and Cl
376 apatites. American Mineralogist, 74, 870-876.
377 Hughes, J.M., Cameron, M., and Crowley, K.D. (1990) Crystal structures of natura ternary apatites:
378 solid solution in the $Ca_5(PO_4)_3X$ (X = F, OH, Cl) system. American Mineralogist, 75, 295-
379 304.
380 Hughes, J.M., Nekvasil, H., Ustunisik, G., Lindsley, D.H., Coraor, A.E., Vaughn, J., Phillips, B.L.,
381 McCubbin, F.M., and Woerner, W.R. (2014) Solid solution in the fluorapatite-chlorapatite
382 binary system: high precision crystal structure refinements of synthetic F-Cl apatite.
383 American Mineralogist, 99, 369-376.
384 Lim, S.C., Baikie, T., Pramana, S.S., Smith, R., and White, T.J. (2011) Apatite metaprism twin
385 angle (φ) as a tool for crystallochemical diagnosis. Journal of Solid State Chemistry, 184,
386 2978-2986.

Liu, J., Huang, X., Liu J., Wang, W., Zhang, F., and Dong, F. (2014) Experimental and model studies on comparisono of As(III and V) removal from synthetic acid mine drainage by bone char. Mineralogical Magazine, 78, 73-89.

Magalhães, M.C.F., and Williams, P.A. (2007) Apatite group minerals: solubility and environmental remediation. In: Letcher, T.M. (ed.) Thermodynamics, Solubility and Environmental Issues, Elsevier, New York, pp. 327-342.

Magnusson, N.H. (1929) The Nordmark ore district. Sveriges Geologiska Undersökning, Ca 13, 98pp (in Swedish)

Pasero, M., Kampf, A.R., Ferraris, C., Pekov, I.V., Rakovan, J., and White, T.J. (2010) Nomenclature of the apatite supergroup minerals. European Journal of Mineralogy, 22, 163-179.

Pouchou, J.L., and Pichoir, F. (1991) Quantitative analysis of homogeneous or stratified microvolumes applying the model "PAP". In K.F.J. Heinrich, D.E. Newbury, Eds., Electron Probe Quantitation, p. 31-75, Plenum Press, New York.

Rakovan, J.F., and Pasteris, G.D. (2015) A Technological Gem: Materials, Medical, and Environmental Mineralogy of Apatite. Elements, 11, 195-200.

Sheldrick, G.M. (2015) Crystal structure refinement with SHELXL. Acta Crystallographica, C71, 3-8.

Wang, K.L., Zhang,Y., and Naab, F.U. (2011) Calibration for IR measurements of OH in apatite. American Mineralogist, 96, 1392-1397.

Wardojo, T.A., and Hwu, S.J. (1996) Chlorapatite: $Ca_5(AsO_4)_3Cl$. Acta Crystallographica, C52, 2959-2960.

White, T.J., and Dong, Z. (2003) Structural derivation and crystal chemistry of apatites. Acta Crystallographica, B59, 1-16.

White, T., Ferraris, C., Kim, J., and Madhavi, S. (2005) Apatite – An adaptive framework structure. In G. Ferraris, S. Merlino, Eds., Micro- and Mesoporous Mineral Phases, 57, p. 307-401, Reviews in Mineralogy and Geochemistry, Mineralogical Society of America, Chantilly, Virginia.

Wilson, A.J.C. (1992) International Tables for Crystallography Volume C. Kluwer, Dordrecht.

418 ## Table captions

419 **Table 1** – Electron-microprobe data (mean of 10 spot analyses, in wt%) of turneaureite, estimated
420 standard deviation (e.s.d.), and atoms per formula unit (apfu), on the basis of 13 anions. H_2O was
421 calculated with the assumption (Cl+F+OH) = 1 apfu.

422 **Table 2** – Crystal data and summary of parameters describing data collection and refinement for
423 turneaureite.

424 **Table 3** – Site occupancy factors (s.o.f.), fractional atom coordinates, and isotropic (*) or
425 equivalent isotropic displacement parameters (in $Å^2$) for turneaureite. U_{eq} is defined as one third of
426 the trace of the orthogonalized U^{ij} tensor.

427 **Table 4** – Anisotropic displacement parameters (in $Å^2$) for turneaureite.

428 **Table 5** – Selected bond distances (in Å) for turneaureite.

429 **Table 6** – Weighted bond valences for turneaureite, in valence units (v.u.).

430

431 ## Figure captions

432 **Fig. 1** – Anion–anion distances (in Å) for column anions. Same labels as in the text. Grey cells
433 indicate configurations not allowed owing to too short interionic distances.

434 **Fig. 2** – Comparison among the anion colums in johnbaumite (a), svabite (b), and turneaureite (c).
435 The *M*2–*M*2 distances are shown. Atoms are drawn as thermal ellipsoids. Symbols: black = *M*2 site;
436 dark grey = O sites; light grey = (OH)-dominant sites; grey = F-dominant sites; white = Cl-
437 dominant sites.

438 **Fig. 3** – Infrared E||E (E||**c**) spectra of turneaureite (thick line) in the O–H stretching region
439 compared with those of johnbaumite (thin broken line) and svabite (thin dotted line) (Biagioni et al.
440 2016).

441

442 **Table 1** – Electron-microprobe data (mean of 10 spot analyses, in wt%) of turneaureite, estimated
443 standard deviation (e.s.d.), and atoms per formula unit (apfu), on the basis of 13 anions. H_2O was
444 calculated with the assumption (Cl+F+OH) = 1 apfu.

Oxide	wt%	range	e.s.d.	apfu
SO_3	0.22	0.02 – 1.10	0.31	0.018
P_2O_5	0.20	0.12 – 0.26	0.08	0.018
V_2O_5	0.01	0.00 – 0.06	0.02	0.001
As_2O_5	51.76	50.27 – 52.40	0.78	2.942
SiO_2	0.06	0.03 – 0.09	0.02	0.007
CaO	41.39	40.45 – 41.89	0.63	4.821
MnO	1.89	1.54 – 3.37	0.65	0.174
SrO	0.12	0.05 – 0.28	0.08	0.008
BaO	0.52	0.11 – 2.38	0.82	0.022
PbO	0.10	0.00 – 0.24	0.08	0.003
Na_2O	0.02	0.00 – 0.06	0.02	0.004
F	0.32	0.11 – 0.56	0.14	0.110
Cl	2.56	2.15 – 2.84	0.21	0.472
$H_2O_{(calc)}$	0.58			0.421
O = F + Cl	–0.71			
Total	99.04			

445

446 **Table 2** – Crystal data and summary of parameters describing data collection and refinement for
447 turneaureite.

448

Crystal data	
Crystal size (mm)	0.23 x 0.23 x 0.10
Cell setting, space group	Hexagonal, $P6_3/m$
a, c (Å)	9.9218(3), 6.8638(2)
V (Å^3)	585.16(4)
Z	2
Data collection and refinement	
Radiation, wavelength (Å)	Mo$K\alpha$, 0.71073
Temperature (K)	298
Detector-to-sample distance (mm)	50
Number of frames	558
Rotation width per frame (°)	0.5
Maximum observed 2θ (°)	65.05
Measured reflections	2720
Unique reflections	753
Reflections with $F_o > 4\sigma(F_o)$	716
R_{int} after absorption correction	0.0156
R_σ	0.0146
Range of h, k, l	$-8 \le h \le 13$ $-15 \le k \le 10$ $-10 \le l \le 5$
R_1 [$F_o > 4\ \sigma(F_o)$]	0.0172
R_1 (all data)	0.0185
wR_2 (on F^2_o)	0.0447
Goof	1.108
Number of l.s. parameters	42
Maximum and minimum residual	0.75 (at 0.56 Å from $M2$) -0.88 (at 0.74 Å from $M2$)

449
450

451 **Table 3** – Site occupancy factors (s.o.f.), fractional atom coordinates, and isotropic (*) or
452 equivalent isotropic displacement parameters (in Å^2) for turneaureite. U_{eq} is defined as one
453 third of the trace of the orthogonalized U^{ij} tensor.

Site	Wyckoff position	s.o.f.	*x*/*a*	*y*/*b*	*z*/*c*	$U_{eq/iso}$
*M*1	4*f*	$Ca_{0.328(3)}Mn_{0.005(3)}$	2/3	1/3	0.00395(8)	0.01344(14)
*M*2	6*h*	$Ca_{0.491(1)}Ba_{0.009(1)}$	0.01102(6)	0.26117(7)	¼	0.02306(18)
T	6*h*	$As_{0.50}$	0.37437(3)	0.40457(3)	¼	0.01006(8)
O1	6*h*	$O_{0.50}$	0.5020(2)	0.3416(2)	¼	0.0198(4)
O2	6*h*	$O_{0.50}$	0.4663(2)	0.6012(2)	¼	0.0171(3)
O3	12*i*	$O_{1.00}$	0.25644(16)	0.34708(18)	0.44470(19)	0.0217(3)
*X*a	2*a*	$(OH)_{0.070}F_{0.018}$	0	0	¼	0.0160(5)*
*X*b	4*e*	$Cl_{0.068}$	0	0	0.3055(6)	0.0160(5)*
*X*c	4*e*	$Cl_{0.010}$	0	0	0.370(4)	0.0160(5)*

454

455

456 **Table 4** – Anisotropic displacement parameters (in Å^2) for turneaureite.

Site	U^{11}	U^{22}	U^{33}	U^{23}	U^{13}	U^{12}
*M*1	0.01587(18)	0.01587(18)	0.0086(2)	0	0	0.00794(9)
*M*2	0.0162(2)	0.0346(3)	0.0117(2)	0	0	0.0077(2)
T	0.01083(11)	0.01054(11)	0.01045(11)	0	0	0.00658(8)
O1	0.0230(9)	0.0338(10)	0.0146(7)	0	0	0.0233(9)
O2	0.0178(8)	0.0098(7)	0.0225(8)	0	0	0.0060(6)
O3	0.0188(6)	0.0351(7)	0.0156(6)	0.0097(6)	0.0066(5)	0.0168(6)

457

458 **Table 5** – Selected bond distances (in Å) for turneaureite.

459

*M*1	O1 (× 3)	2.3800(13)	*M*2	O3 (× 2)	2.3159(13)	*T*	O1	1.6681(18)
	O2 (× 3)	2.4609(14)		O2	2.345(2)		O3 (× 2)	1.6772(13)
	O3 (× 3)	2.8953(16)		O3 (× 2)	2.5232(15)		O2	1.6909(17)
				*X*a	2.5384(7)			
				*X*b	2.5669(9)			
				Xc	2.669(9)			
				O1	3.121(2)			
	<*M*1–O>	2.579		<*M*2–O>	2.529		<*T*–O>	1.678

460

461

This is a preprint, the final version is subject to change, of the American Mineralogist (MSA)
Cite as Authors (Year) Title. American Mineralogist, in press.
(DOI will not work until issue is live.) DOI: http://dx.doi.org/10.2138/am-2017-6041

462 **Table 6** – Weighted bond valences for turneaureite, in valence units (v.u.).

Site	O1	O2	O3	*X*a	*X*b	*X*c	Σ cations
*M*1	$^{3x\rightarrow}0.32^{\times 2\downarrow}$	$^{3x\rightarrow}0.26^{\times 2\downarrow}$	$^{3x\rightarrow}0.08$				1.98
*M*2	0.04	0.36	$^{2x\rightarrow}0.39$ $^{2x\rightarrow}0.22$	$0.11^{\times 3\downarrow}$	$0.25^{\times 3\downarrow}$	$0.02^{x3\downarrow}$	2.00
T	1.31	1.23	$^{2x\rightarrow}1.28$				5.10
Σ anions	1.99	2.11	1.97	0.33	0.75	0.06	

Note: left and right superscripts indicates the number of equivalent bonds involving cations and anions, respectively. For sites with mixed occupancy, the bond valences have been weighted according to the proposed site population: *M*1 = $Ca_{1.00}$; *M*2 = $Ca_{0.93}Mn_{0.06}Ba_{0.01}$.

463

464

465

466 **Fig. 1** – Anion–anion distances (in Å) for column anions. Same labels as in the text. Grey cells
467 indicate configurations not allowed owing to too short interionic distances.

Anion associated with mirror plane at z = ¾

Anion associated with mirror plane at z = ¼

	Xa	Xb_a	Xb_b	Xc_a	Xc_b
Xa	3.43	3.81	3.05	4.26	2.61
Xb_a	3.05	3.43	2.67	3.88	2.23
Xb_b	3.81	4.19	3.43	4.64	2.99
Xc_a	2.61	2.99	2.23	3.43	1.78
Xc_b	4.26	4.64	3.88	5.08	3.43

468

469

Fig. 2 – Comparison among the anion colums in johnbaumite (a), svabite (b), and turneaureite (c). The *M*2–*M*2 distances are shown. Atoms are drawn as thermal ellipsoids. Symbols: black = *M*2 site; dark grey = O sites; light grey = (OH)-dominant sites; grey = F-dominant sites; white = Cl-dominant sites.

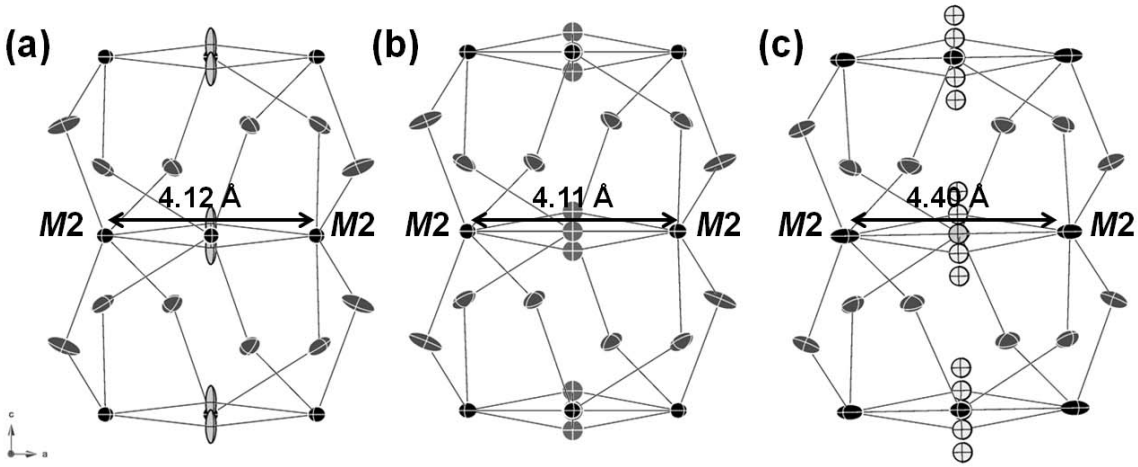

476 **Fig. 3** – Infrared E||E (E||**c**) spectra of turneaureite (thick line) in the O–H stretching region
477 compared with those of johnbaumite (thin broken line) and svabite (thin dotted line) (Biagioni et al.
478 2016).

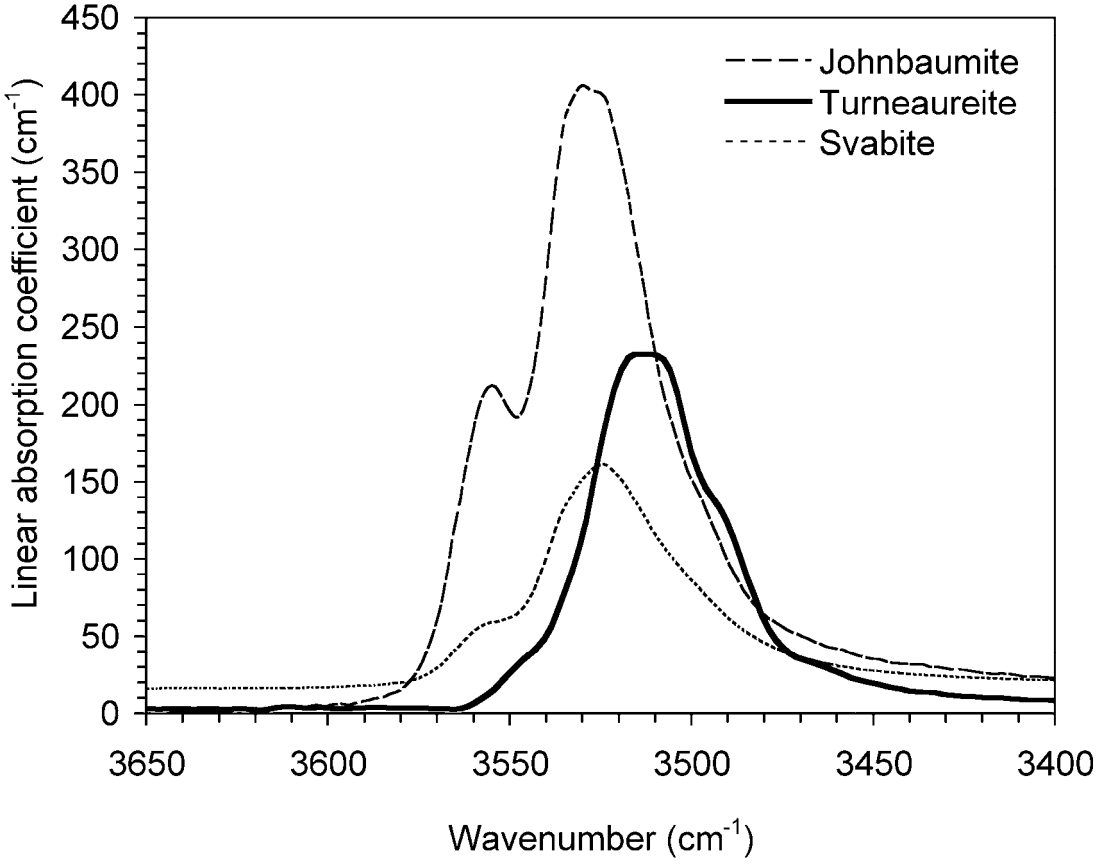

479

480

This is a preprint, the final version is subject to change, of the American Mineralogist (MSA)
Cite as Authors (Year) Title. American Mineralogist, in press.
(DOI will not work until issue is live.) DOI: http://dx.doi.org/10.2138/am-2017-6041

Anion associated with mirror plane at z = ¾

Anion associated with mirror plane at z = ¼

	Xa	Xb_a	Xb_b	Xc_a	Xc_b
Xa	3.43	3.81	3.05	4.26	2.61
Xb_a	3.05	3.43	2.67	3.88	2.23
Xb_b	3.81	4.19	3.43	4.64	2.99
Xc_a	2.61	2.99	2.23	3.43	1.78
Xc_b	4.26	4.64	3.88	5.08	3.43

This is a preprint, the final version is subject to change, of the American Mineralogist (MSA)
Cite as Authors (Year) Title. American Mineralogist, in press.
(DOI will not work until issue is live.) DOI: http://dx.doi.org/10.2138/am-2017-6041

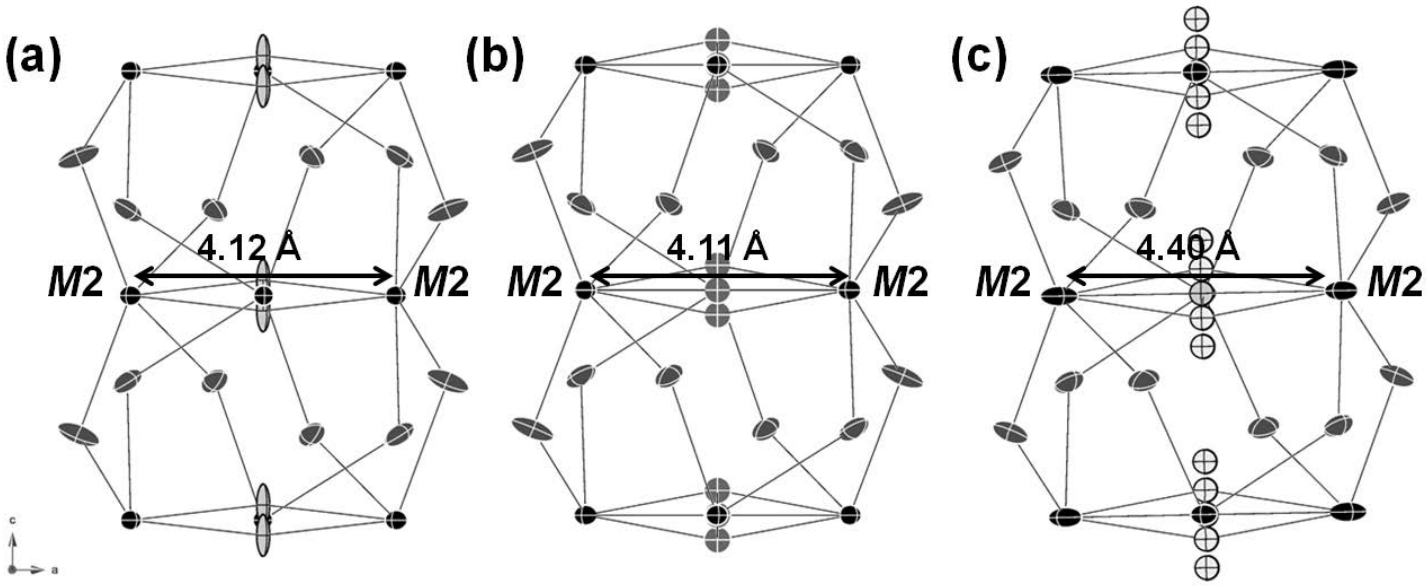

This is a preprint, the final version is subject to change, of the American Mineralogist (MSA)
Cite as Authors (Year) Title. American Mineralogist, in press.
(DOI will not work until issue is live.) DOI: http://dx.doi.org/10.2138/am-2017-6041